Ab Initio Study of Radical Reactions: Cyclization Pathways for the Butylbenzene Radical (II)

V. Van Speybroeck,* Y. Borremans,† D. Van Neck, and M. Waroquier

Laboratory of Theoretical Physics, Universiteit Gent, Proeftuinstraat 86, B-9000 Gent, Belgium

S. Wauters,‡ M. Saeys, and G. B. Marin

Laboratorium voor Petrochemische Techniek, Universiteit Gent, Krijgslaan 281-S5, B-9000 Gent, Belgium

Ab initio density functional theory calculations are presented on some model reactions involved in coke formation during the thermal cracking of hydrocarbons. The reactions under consideration are different cyclization pathways for the butylbenzene radical, which can lead to a further growth of the coke layer. This study enables us to gain more microscopic insight into the mechanistic and kinetic aspects of the reactions. Special attention is paid to the exact treatment of internal rotations and their impact on the kinetic parameters. Pre-exponential factors are very sensitive to the accuracy of constructing the microscopic partition functions. In particular, the relative importance of cyclization toward five and six-membered rings is studied on the basis of the calculated rate constants and concentration profiles of the reactants. The influence of the size of the ring and of the relative stability of the primary and secondary butylbenzene radical on the cyclization reaction is discussed. The activation energy for the formation of six-membered rings is approximately 30 kJ/mol lower than that for five-ring formation. The predicted values for the kinetic parameters enable us to validate some basic assumptions on coke formation. The calculations as presented here are especially important for complex reaction schemes, for which experimental data are not always available.

1. Introduction

Thermal cracking of hydrocarbons is one of the main processes for the production of light olefins such as ethene. In today's operation of a plant for thermal cracking, simulation models play a very important role. These models comprise two major parts: a mathematical model of the reactor itself and a kinetic model which describes the changes in the reactor and the rate at which they occur. The thermal cracking of hydrocarbons is known to proceed through a free-radical mechanism. Small radicals are formed via C−C bond breaking and react further via abstraction and addition reactions. Decomposition of the formed radicals results in the desired gas-phase olefins.[1] During the thermal cracking, a carbonaceous deposit, coke, is formed on the inner walls of the reactor tubes. Radicals of the gas phase create radical species on the coke surface at which olefins can add. Cyclization and dehydrogenation lead to further growth of the coke layer by incorporation of the carbon atoms. This coke layer has a negative influence on the efficiency of the cracking unit.[2]

The most difficult part of constructing a kinetic model consists of assigning values to the rate constants of the individual reactions. For every reaction, this requires a value for the frequency factor and the activation energy. Taking into account the fact that the reaction scheme contains some 500 reactions in which some 30 molecular species and 30 radicals are involved, it is quite obvious that the determination of some thousand parameters by means of regression of experimental product distributions is both practically infeasible and fundamentally undesirable. A possible way of dealing with this problem is to use theoretical methods to predict the kinetic parameters of the basic reactions occurring in the reaction scheme. Considerable progress in this respect has been made by Benson and co-workers.[3] These methods allow estimates of the rate coefficients on a semiempirical basis, from the structure and energetics of the molecule or radical considered. Another approach based on transition state theory (TST)[4] was used by Willems and co-workers[5] to obtain semiquantitative predictions for the pre-exponential factor and activation energies of gas-phase reactions. The structure of the transition state was based on chemical intuition. As indispensable as these methods are from the practical viewpoint of modeling, their empirical input limits their use for quantitative microscopic predictions, and their relationship with fundamental molecular properties, such as the potential energy surface, is indirect. To obtain more insight into the microscopic scale of the reaction, ab initio calculations can give a valuable contribution. Because of increasing capabilities of computers and continuous optimization of available numerical methods, theoretical calculations with high accuracy on industrial important processes become within the frame of applicability. Recently, ab initio calculations have been carried out to calculate energies and frequency factors within the framework of TST for the addition of *n*-alkyl radicals to ethene.[6−8] Also, Richter and co-workers[9] performed detailed kinetic studies on the growth of small polycyclic aromatic hydrocarbons.

In a previous paper of the authors,[10] the addition reaction of the ethylbenzene radical to ethene, the gas-phase analogue for one of the main reactions of the coke formation network,[11] has been studied on a high ab initio level. Accurate predictions of the Arrhenius parameters were obtained by means of TST. All

* To whom all correspondence should be addressed. Fax: 32 (0)9264 65 42. E-mail: veronique.vanspeybroeck@rug.ac.be.

† Current address: Dow Benelux N.V., Process Development & Control Department, PO Box 48-4530 AA Terneuzen, Belgium.

‡ Current address: BASF, Scheldelaan 600 Haven 725, 2040 Antwerpen, Belgium.

10.1021/jp010992a CCC: $20.00
Published on Web 07/12/2001

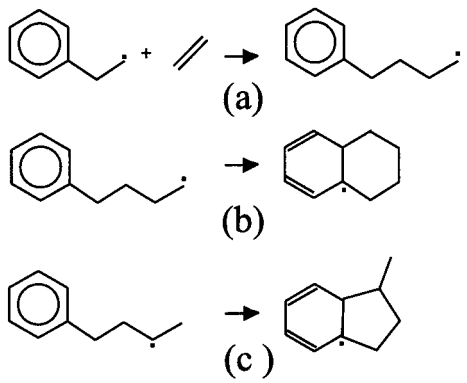

Figure 1. (a) Addition of the ethylbenzene radical. (b, c) Cyclization pathways for the butylbenzene radical.

necessary microscopic quantities like geometries, ground-state energies, and frequencies for the evaluation of molecular partition functions were obtained by performing a detailed conformational and frequency analysis of reactants, products, and activated complexes. One of the main difficulties in the rigorous analysis of long chain hydrocarbons is the presence of one or more internal rotors.[12] These torsional motions are generally opposed by a potential barrier depending on the structural features inhibiting the rotation. At low temperatures, the internal rotors can lead to good approximations in terms of a harmonic oscillator model. At elevated temperatures encountered in the thermal cracking unit, the average energy of the molecule largely exceeds that of the barrier, and the torsional motion can to a good extent be modeled by a free rotor. The intermediate case between the two extreme regimes is the one of a hindered internal rotor. In our study on the addition reaction of the ethylbenzene radical to ethene,[10] it was found that an explicit treatment of internal rotations on a quantum mechanical basis may alter in a considerable way the theoretically predicted values of the Arrhenius parameters and especially the value of the frequency factor. The activation energy is mainly determined by the difference in ground-state energies between the activated complex and the reactants. This feature is not surprising because in the internal rotation approximation the number of states in which the molecule can reside due to thermal agitation is much larger than that of the harmonic oscillator approach.[10]

In this paper, standard ab initio density functional theory (DFT)[13] calculations are performed to analyze in detail different cyclization pathways for the butylbenzene radical. Two possible pathways are studied as schematically depicted in Figure 1b,c. These reactions are gas-phase analogues for basic reactions of the coke formation, which can lead to a further growth of the coke layer. It is a well-known feature of chemistry[14] that the stability of radicals is increased in the order of primary, secondary, and tertiary radicals. Therefore, primary radicals can rearrange themselves to the more stable secondary or even better tertiary radical through the hydrogen shift. The isomerization of the primary to the secondary radical can also occur via successive hydrogen abstractions. In this way, the primary butylbenzene radical, which is formed as a direct product of the radical addition reaction (Figure 1a), can rearrange toward the secondary butylbenzene radical. Both primary and secondary radicals can undergo a ring closure reaction to form either a five-membered or six-membered ring. In this study, we investigate the radical cyclization preference by calculating kinetic parameters for the competitive pathways by means of TST. In complete analogy with the study performed on the addition reaction,[10] we also perform a detailed conformational analysis of the secondary butylbenzene radical. Special attention is paid to the exact quantum-mechanical treatment of internal rotations. The associated potential barriers for these internal motions are obtained by high-level ab initio calculations. Furthermore, accurate geometries and frequencies are calculated for the different transition states and products. These quantities serve as an input for the microscopic partition functions that can be related to the interesting macroscopic parameters such as the frequency factor and the activation energy. On the basis of the theoretical predicted kinetic values, some basic assumptions of the kinetic model describing coke formation can be established.

2. Computational Details

Transition state theory[4] is an adequate method for the evaluation of macroscopic kinetic quantities of chemical reactions. It has proven its success in many studies for the quantitative prediction of kinetic parameters.[6−8,10,15] In TST, the rate coefficient for the reaction A → B is given by

$$k(T) = \frac{k_B T}{h} \frac{q_{\ddagger}}{q_A} e^{-\Delta E_0/(k_B T)} \qquad (1)$$

where k_B represents the Boltzman's constant, T is the temperature, h is Planck's constant, ΔE_0 (for further reference called the critical energy) represents the molecular energy difference at the absolute zero between the activated complex and the reactant (with inclusion of the zero-point vibrational energies), and $q_{\ddagger}$ and q_A are the molecular partition functions of the transition state and reactant, respectively. The molecular properties, such as geometries (moments of inertia), ground-state energies, and frequencies, required for the evaluation of the partition functions and the critical energy ΔE_0 are obtained by ab initio molecular calculations.

All ab initio calculations were carried out with the GAUSSIAN 98 software package[16] within the DFT framework[13] by using the Becke's three parameter hybrid B3LYP functional.[17] The molecular orbitals are expanded in the triple-ζ 6-311G basis augmented with single first d and p polarization functions.[18] Several studies[19−21] have indicated that B3LYP and even Hartree−Fock (HF) methods are sufficiently accurate for the estimation of the relative stabilities of different conformers and for the calculation of the potential energy profile for internal rotation, especially when large basis sets including polarization functions are used. According to specific studies on similar radical reactions,[8] the B3LYP method gives a reliable and quantitatively good description of geometries, frequencies, reaction barriers, and pre-exponential factors. In this case where the system of interest is quite large, B3LYP provides a viable alternative for more computational-intensive methods like CBS,[22] G2,[23] or CBS−RAD[24] procedures. Energy minima were located by full geometry optimizations with the Berny algorithm.[25,26] The transition structures were located according to the following procedure: at the first stage, all variables but the reaction coordinate are optimized while the reaction coordinate was varied stepwise. The maximum of this linear transit served as the starting structure of a transition state optimization using the transit-guided quasi-Newton (STQN) method.[25,26]

The vibrational frequencies of the optimized structures are also calculated at the same level of theory. It is well-known that the B3LYP harmonic vibrational frequencies are systematically larger than the observed experimental frequencies. The overestimation, however, is found to be relatively uniform, and as a result, generic frequency scaling factors are often applied. A scaling factor of 0.9614 is applied to the frequencies in the

evaluation of the partition functions,[27] while the zero-point vibrational energies are scaled with 0.9806.[27]

By analyzing the vibrational spectrum of the molecule and in particular the low vibrational modes, it is possible to identify some motions that correspond to internal rotations. In this paper, all internal rotations are treated in an exact quantum-mechanical way but uncoupled. The rotational energy levels of all internal motions are calculated by solving the appropriate one-dimensional Schrödinger equation using the same numerical algorithm as that outlined in ref 10:

$$-\frac{\hbar^2}{2I_m}\frac{\partial^2\psi_{km}(\phi_1,\phi_2,...,\phi_M)}{\partial\phi_m^2} + V(\phi_1,\phi_2,...,\phi_M)\psi_{km}(\phi_1,\phi_2,...,\phi_M) = \epsilon_k(m)\psi_{km}(\phi_1,\phi_2,...,\phi_M) \quad \text{for } m = 1, ..., M \tag{2}$$

where ψ_{km} represents the rotational wave function and $\epsilon_k(m)$ are the rotational energy levels for the internal rotation m defined by the dihedral angle ϕ_m. I_m stands for the reduced moment of inertia for the rotation of the mth top. The rotational potential $V(\phi_1, \phi_2, ..., \phi_M)$ is in principle not separable into the various torsional angles. We apply the following approximative scheme to reduce the dimensionality of the potential: through the stationary points along the rotational potential—corresponding to fully optimized conformers—a k_{max}-Fourier expansion is fit:

$$V_m(\phi_m) = \sum_{k=1}^{k_{max}} \frac{1}{2} V_{mk}(1 - \cos(k\phi_m)) \tag{3}$$

We always have more than one harmonic, and hence, the standard solution procedure available for one harmonic cannot be used.[28] We apply a computational procedure based on solving the Schrödinger equation on a discretized angular grid, as outlined in ref 10. Once the energy levels $\epsilon_k(m)$ are evaluated for each internal rotation m, the partition functions $q_{rot,int}$ can be constructed by the product over the M individual internal rotation partition functions

$$q_{rot,int,m} = \frac{1}{\sigma_{int}}\sum_k g_k(m)\exp\left(-\frac{\epsilon_k(m)}{k_B T}\right) \tag{4}$$

with $g_k(m)$ being the degeneracy of the rotational energy level $\epsilon_k(m)$ for the mth top and σ_{int} the symmetry number of the internal rotation. The number of eigenstates chosen is high enough to get sufficient convergence of the rotational partition function.

In this way, we achieve one of the main goals of this reaction study: we have established a microscopic description of the rate constant versus temperature according to eq 1. Following the Arrhenius rate law, the reaction rate constant is given by

$$k(T) = Ae^{-E_a/(RT)} \tag{5}$$

with R being the universal gas constant, A the pre-exponential factor or frequency factor, and E_a the activation energy, which are assumed to be temperature-independent. On the other hand, in TST, the kinetic parameters A and E_a are in principle temperature-dependent due to their construction (by means of partition functions). We found (section 3.3) that for the reaction under study in the considered temperature range, the Arrhenius rate law models very good the temperature dependence of the rate constant. Using eq 1, we calculate the rate coefficients at different temperatures. The two kinetic parameters are then computed by a least-squares fit from a set of rate coefficients at different temperatures determined through eq 1. The results are discussed in section 3.

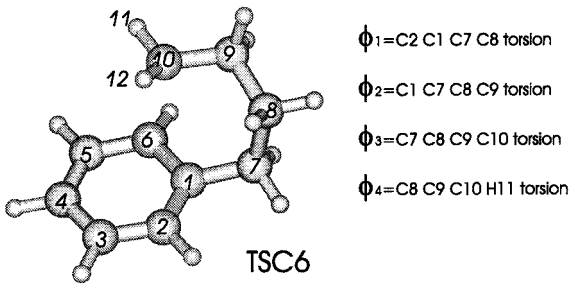

Figure 2. Transition state for cyclization of the primary butylbenzene radical.

3. Results and Discussion

3.1. Cyclization of the Primary Butylbenzene Radical. *3.1.1. Reactants.* The reactant for this ring closure reaction is the primary butylbenzene radical. The conformational analysis of this radical has been studied in great detail in ref 10. In this paper, we only note those results which are needed for the transparency of the present work. For the primary butylbenzene radical, four internal rotations were identified, corresponding to variations of the dihedral angles ϕ_1, ϕ_2, ϕ_3, and ϕ_4, as indicated in Figure 2. The butylbenzene radical has five main local minima on the potential energy surface, which are mainly generated by varying the two rotational angles ϕ_2 and ϕ_3. Details about the geometries and energies of the different conformers can be found in ref 10. All internal rotations are treated according to the scheme explained in section 2. The rotational potential is obtained by a Fourier fitting procedure through all stationary points—determined by full geometry optimizations—in terms of the different torsional angles. The results are given in ref 10.

3.1.2. Transition State. Geometries. To locate the transition structure, we followed the procedure as outlined in section 2. The reaction coordinate was approximated by the distance C_6-C_{10} of the forming bond starting from the BB5 conformer (the folded conformation as defined in ref 10). Figure 2 shows the structure of the optimized transition structure, which will be called the TSC6 conformer for later reference. The forming C−C bond reaches a distance of 2.180 Å in the activated complex. In addition, the transition structure for cyclization predicts a nonplanarity of the benzene ring of 7.6°, given by the dihedral angle $C_1C_6C_5C_4$ at the center C_6 where the butylchain attacks. In order for the reaction to take place, the aromaticity of the benzene ring must be broken, and the C_6 center transforms from a trigonal to a tetrahedral carbon center. Also, the deviation from planarity at the ending radical carbon center C_{10} increases with respect to the similar property in the BB5 conformer: the improper torsion angle $C_9C_{10}H_{11}H_{12}$ reaches values of −142.534° and −174.0°, respectively, in the TSC6 and BB5 conformers. This is an indication for the transformation of C_{10} carbon center from an sp^2 hybridization in the reactant to an sp^3 hybridization in the product state. The dihedral angles ϕ_1, ϕ_2, ϕ_3, and ϕ_4 reach values of −101.074°, −56.533°, −61.137°, and −166.495° respectively.

Vibrational Analysis. The transition state has one imaginary frequency (−491.36 cm^{-1}), which can be associated with a translational or loose vibrational motion along the reaction coordinate. A set of low-lying vibrational frequencies are located at $\nu_{p1} = 105.18$, $\nu_{p2} = 129.959$, $\nu_{p3} = 271.714$, and $\nu_{sk} = 105.18$

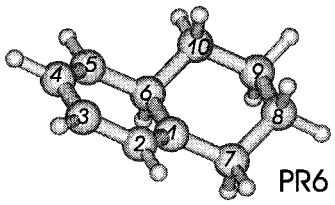

Figure 3. Product state of the cyclization of the primary butylbenzene radical.

cm^{-1}. Inspecting the associated motions for ν_{p1}, ν_{p2}, and ν_{p3} teaches that they correspond to small variations of the torsional angles ϕ_1, ϕ_2, and ϕ_3. However, these motions cannot be regarded as pure internal rotations about a single bond but feel an additional steric hindrance by the forming CC distance that remains almost constant. Such motions are often called ring-puckering vibrations or pseudorotations.[28] The associated potential barriers can be expected to be relatively high due to the large steric hindrance caused by the nearby aromatic ring. Therefore, a treatment of these motions in the harmonic oscillator approximation is justified. The methylene rotation which was also present in the BB5 conformer does not appear here due to the presence of the forming CC bond. The other low-lying frequency ν_{sk} is a skeletal vibration. These type of motions arise in large structures, and their frequency is often on the same order of magnitude as those of the internal rotations. The higher the mass of the cluster involved in the skeletal motion is, the lower the corresponding frequency ν_{sk} will be. Because of their complexity, we will treat them in the harmonic oscillator approximation.

3.1.3. Product State. Geometries. The optimized structure for the product state is shown in Figure 3. This structure will be referred as the PR6 conformer for later reference. The product of the cyclization reaction is a fused-ring system where the original butylchain and two carbon atoms originating from the former aromatic ring join to form a six-membered ring. The new formed ring structure can be compared with a cyclohexane ring in a chair form apart from the radical center at C_1. The C_6 center exhibits in the new structure after cyclization to sp^3 hybridization. This feature is reflected in enlarged bond lengths of the connecting carbon−carbon bonds ($C_5-C_6 = 1.501$ Å, $C_6-C_1 = 1.511$ Å) compared with the bond lengths of a single benzene ring (1.397 Å).[29] The value of the C_6-C_{10} bond (1.561 Å) is in very good agreement with analogous values for single carbon−carbon bonds (propane, 1.541 Å; ethane, 1.538 Å; propene, 1.520 Å[29]). The planarity of the former aromatic ring is almost recovered in the PR6 conformation ($C_1C_6C_5C_4 = 0.8°$), although the aromaticity can only be reestablished by abstraction of an hydrogen atom at the C_6 center or by emission of an hydrogen atom under the influence of the neighboring radical center.

The C_1 carbon center exhibits an sp^2 hybridization, and the connecting bonds C_1-C_2 (1.366 Å) and C_1-C_7 (1.503 Å) turn out to be shorter than those in an aromatic bond and a single carbon−carbon bond, respectively. Also, this center shows small deviations from planarity ($C_2C_1C_6C_7 = 178.0°$).

The CC bond lengths in the new formed ring reach typically values of single CC carbon bonds ($C_7-C_8 = 1.543$ Å, $C_8-C_9 = 1.535$ Å, $C_9-C_{10} = 1.534$ Å), and the bond angles of the carbon atoms of the former butylchain all reach values of approximately 110°.

Vibrational Analysis. The lowest frequency in the PR6 conformer reaches a value of $\nu_b = 96.26$ cm^{-1} and corresponds to a bending motion of the two fused rings toward each other. The other low-lying frequencies originate either from skeletal vibrations, which are typically present in large structures such as the ones considered here, or to pseudorotation in the newly formed ring structure. Because of the complexity of these modes, we will treat them in the harmonic oscillator approximation.

TABLE 1: Geometrical Parameters for the Stable Conformers of the Secondary Butylbenzene Radical[a]

	ϕ_1	ϕ_2	ϕ_3	ϕ_4	E_0^{rel}
BBsec1	−89.0	179.5	166.6	−45.7	0.0
BBsec2	−75.4	−64.3	−160.9	−167.1	2.24
BBsec3	−88.5	180.0	−83.0	78.7	0.95
BBsec4	−83.3	−66.2	−84.1	−41.9	3.61
BBsec5	−84.3	−65.4	109.1	47.8	3.44

[a] ϕ_1, ϕ_2, ϕ_3, and ϕ_4 are the torsional angles as defined in Figure 2. E_0^{rel} is the total binding energy (kJ/mol) relative to the BBsec1 conformer (−388.94224 au) with the exclusion of ZPE.

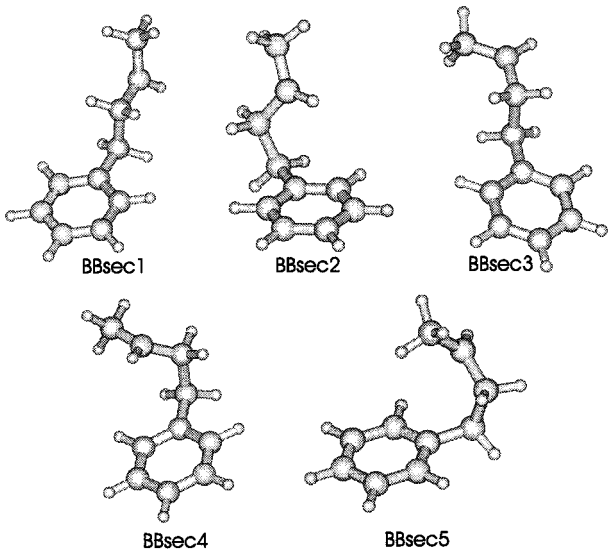

Figure 4. Stable conformers of the secondary butylbenzene radical.

3.2. Cyclization of the Secondary Butylbenzene Radical. Another possible cyclization pathway for the butylbenzene radical is the one where a secondary radical forms a five-membered ring during a ring-closure reaction (as displayed in Figure 1c). The secondary radical can be directly formed from the primary radical by a hydrogen shift, although a theoretical study by Viskolcz et al.[30] shows that such hydrogen shift reactions are usually highly activated. The isomerization of the primary to the secondary radical can also occur via successive hydrogen abstractions. Organic radicals are usually more stable in the order of primary, secondary, and tertiary radicals. The stability of organic radicals is usually measured through the readiness of their formation by a hydrogen abstraction reaction.[31] For example, the reactivity of primary, secondary, and tertiary positions in aliphatic hydrocarbons toward hydrogen abstraction by the methyl radical is 1:4.3:46.[32]

3.2.1. Reactant. Geometries. The reactant in this case is the secondary butylbenzene radical. A strong conformational analogy can be expected between the primary and secondary butylbenzene radical. Five stable minima are located on the potential energy surface. Geometrical parameters and binding energies are listed in Table 1. For each, the angle between the butylchain and the benzene plane is approximately 90°, and the combination of gauche and anti orientations of the remaining CCCC torsions in the butylchain generate five stable minima. They are displayed in Figure 4. We define the torsional angles ϕ_1, ϕ_2, ϕ_3, and ϕ_4 as indicated in Figure 5. The geometrical

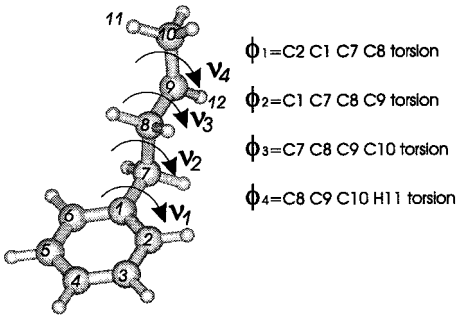

Figure 5. Definition of torsional angles in the secondary butylbenzene radical.

TABLE 2: Lowest Vibrational Frequencies (in cm^{-1}) for the Secondary Butylbenzene Radical

	BBsec1	BBsec2	BBsec3	BBsec4	BBsec5
ν_1	33.8	37.0	30.6	33.6	25.9
ν_2	69.9	67.7	67.0	135.3	92.4
ν_3	57.1	59.2	50.7	96.5	44.3
ν_4	115.3	118.5	89.9	37.9	58.5
ν_{sk}	78.5	156.7	113.3	62.0	130.7

values for these four dihedral angles, together with the total binding energies relative to the BBsec1 conformer, are given in Table 1.

The lowest-energy conformer is the BBsec1 conformer, which is characterized by an anti orientation about both the C_7-C_8 and C_8-C_9 bonds. This conformer no longer exhibits C_s symmetry, which was found for the primary butylbenzene radical. This is due to the presence of the radical center at C_9. The only symmetry operation which is present for all conformers of both primary and secondary butylbenzene radicals is the double switch operation

$$\hat{V}V(\phi_2, \phi_3) = V(-\phi_2, -\phi_3) \tag{6}$$

All other conformers show a strong analogy with the primary radical: BBsec3 is also an anti conformer for the orientation of the side chain about the C_7-C_8 bond but has a gauche orientation about the C_8-C_9 bond. BBsec2, BBsec4, and BBsec5 are gauche conformers about the C_7-C_8 bond and are further split up by anti and two possible staggered orientations of the ending CH_3CH group around the C_8-C_9 bond.

Since the C_9 carbon center has an sp^2 hybridization, the deviations from exact gauche and anti orientations are larger than those of the primary butylbenzene radical. Another remarkable difference with respect to the primary radical is that the BBsec5 radical is slightly stabilized over the BBsec4 conformer. The radical center probably has a positive overlap with the π-conjugated system of the aromatic ring.

Vibrational Analysis. The identification of all internal rotations requires a vibrational analysis of all structures and in particular of the low vibrational modes. Table 2 lists the lowest vibrational frequencies for all optimized structures. The vibrations of the most stable conformer BBsec1 are studied in more detail. ν_1, ν_2, ν_3, and ν_4 can be associated with internal motions resulting from variations of the dihedral angles ϕ_1, ϕ_2, ϕ_3, and ϕ_4. ν_1 corresponds to a rotation of the butylchain about the aromatic ring, while the frequencies ν_2, ν_3, and ν_4 are associated with the rotations about the C_7-C_8, C_8-C_9, and C_9-C_{10} bond, respectively. The frequency ν_{sk} corresponds to a skeletal vibration, more precisely, a bending mode of the butylchain toward the aromatic ring.

Torsional Potentials. The rotational potentials for each of the internal rotations present in the secondary butylbenzene radical are determined by fitting a Fourier expansion through the stationary points—determined by full geometry optimizations—as explained in section 2. The resulting torsional potentials for the four internal rotations are displayed in Figure 6.

The rotation about the C_1-C_7 bond has two stationary points in a period of π. The minimum-energy configuration corresponds with the BBsec1 conformer that is characterized by an orthogonal orientation of the butylchain toward the aromatic ring. The maximum-energy configuration corresponds to a geometry in which the butylchain has an almost planar orientation toward the aromatic ring. Unlike the situation for the primary butylbenzene radical, this conformation does not exhibit the C_s symmetry, due to the presence of the radical center at C_9 that slightly deviates from exact planarity. The reduced moment of inertia for this motion amounts to 123.61 au. The rotational energy levels are displayed in Figure 6a. In this particular case, the energy levels are doubly degenerate because of the periodicity of π combined with the high inertial moment ($\hbar^2/(2I_m) = 0.0058$ kJ/mol) compared with the potential barrier (5.59 kJ/mol). The symmetry number for this specific rotation is 2 ($\sigma_{int} = 2$) since for every conformation a symmetrically equivalent structure can be found by applying a rotation of 180° of the butylchain.

For the rotation about the C_7-C_8 bond, the rotational potential is very similar to the well-known CCCC rotational profile found in *n*-butane. The minima correspond to anti and gauche orientations of the rotating groups, whereas the maxima are associated with eclipsed conformations. The reduced moment of inertia for this rotation amounts to 185.08 au.

The rotation about the C_8-C_9 bond actually corresponds to a rotation-inversion process since the C_9 carbon center has an sp^2 hybridization. The Newman projections for this internal motion are displayed in Figure 7. Because of the nonplanarity of the radical center, we need two torsional angles $\phi_3 = C_7C_8C_9C_{10}$ and $\phi'_3 = C_7C_8C_9H_{12}$ in order to determine unambiguously the combined rotation-inversion process. However, the mechanism is better described by introducing a new parameter θ_3 related to ϕ_3 and ϕ'_3 by the relation $\theta_3 = (\phi_3 + \phi'_3)/2$. The BBsec1 conformer is the energetically most favored structure. Inversion at the radical center generates a symmetrically equivalent geometry with the same energy. The maximum-energy conformation lying between these two energy minima is the BBsec1−BBsec1 conformer and has a planar radical center. The next stable minimum is the BBsec3 conformer. For this structure, no additional minimum appears by inversion at the radical center due to large steric hindrance. The resulting potential in function of θ_3 is displayed in Figure 6c. It has only four minima in a period of 2π, while one could normally expect six minima for a center with sp^2 hybridization. The missing minima are prevented by large steric hindrance of the methyl group attached at the C_9 carbon atom, and the potential energy differences are dominated by the variation of the angle ϕ_3. Because of the specific behavior of the potential, we extend the three-term Fourier expansion (conform eq 3) with a single $\sin(12\theta)$ which only contributes in the range from −7.5° and 7.5° to simulate the behavior around $\theta = 0°$. This additional contribution has a very small effect on the generated potential and the corresponding rotational energy levels.

The rotational potential for the rotation about the C_9-C_{10} bond has a period of $\pi/3$. This could be expected since the ending methyl group is a symmetric top with 3-fold symmetry. The associated symmetry number to be used in the evaluation of the partition function is 3 ($\sigma_{int} = 3$).

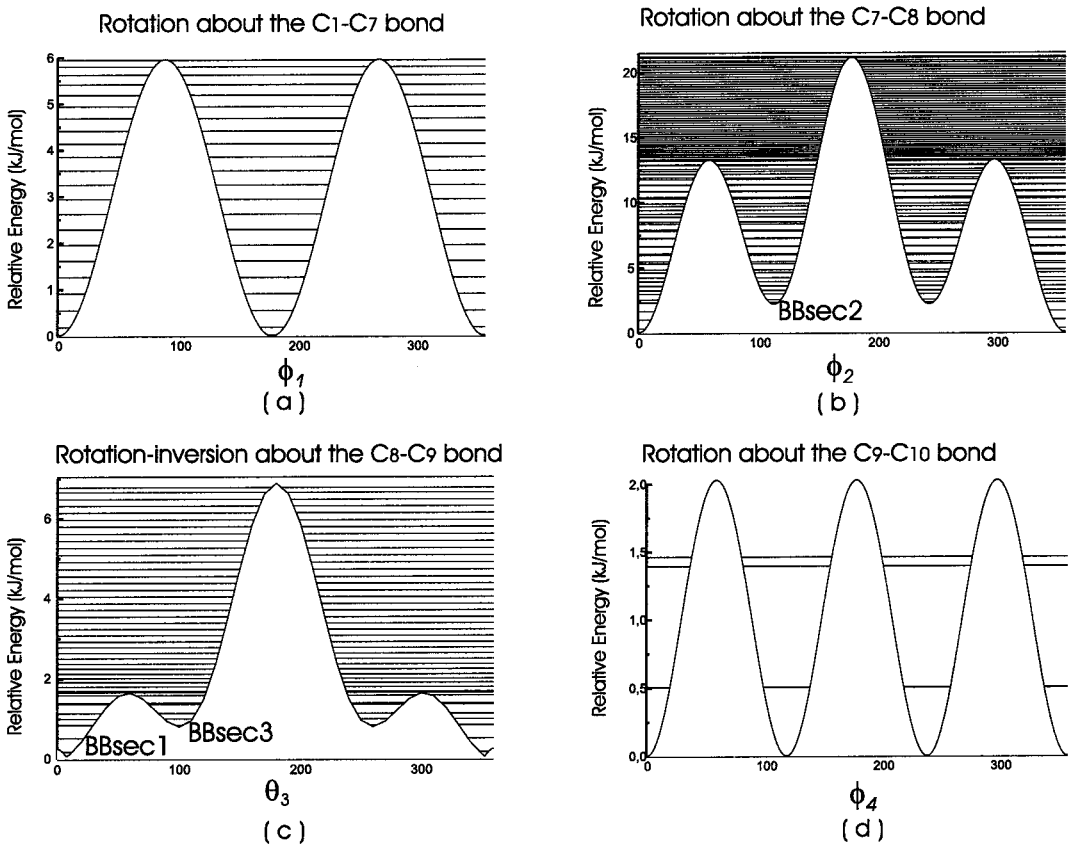

Figure 6. Rotational potentials for the torsional motions in the secondary butylbenzene radical. The energies are relative to that of the BBsec1 conformer. The torsional angles are relative to the equilibrium geometry of the BBsec1 conformer.

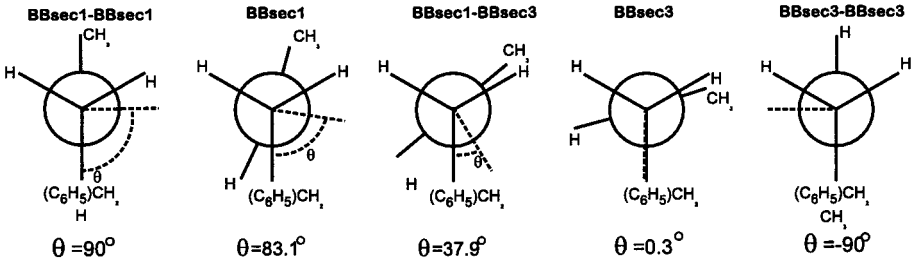

Figure 7. Newman projections of the rotation inversion about the C_8-C_9 bond in the BBsec1 conformer.

The results of Fourier fitting procedure are summarized in Table 3.

3.2.2. Transition State. Geometries. The transition state for cyclization of the secondary butylbenzene radical is shown in Figure 8. The structure was located by gradually decreasing the C_6C_9 distance. The maximum of this linear transit served as an initial guess for a full geometry optimization of the transition state. For later reference, this state will be referred to as the TSC5 conformer. The distance of the forming carbon−carbon bond amounts to 2.1135 Å. The former aromatic ring deviates from its planar structure ($C_5C_6C_1C_2 = -3.978°$, $C_1C_2C_3C_4 = -1.617°$, $C_2C_3C_4C_5 = 1.775°$), since the C_6 carbon atom transforms from an sp^2 toward an sp^3 center during the cyclization reaction. The other carbon atom participating in the forming CC bond, namely, the former radical center C_9, evolves from a trigonal toward a tetrahedral center during the cyclization reaction. This is characterized by the deviation from planarity of the carbon center C_9 (the improper torsion angle $C_8C_9C_{10}H_{12} = 140.237°$) and the bond angles with its neighboring atoms ($C_{10}C_9H_{12} = 114.394°$, $H_{12}C_9C_8 = 114.92°$, $C_{10}C_9C_8 = 118.236°$).

Vibrational Analysis. The TSC5 conformer is characterized by one imaginary frequency (-531.89 cm^{-1}), corresponding to a loose vibrational motion along the forming CC bond. Also, some other low vibrational frequencies are present namely $\nu_{p1} = 57.4$, $\nu_{p2} = 113.3$, $\nu_{p3} = 197.6$, and $\nu_4 = 204.3$ cm^{-1}. The motions corresponding to ν_{p1}, ν_{p2}, and ν_{p3} can be identified as either skeletal motions or ring-puckering vibrations of the forming ring. The only vibration that can be identified as a pure internal rotation is the rotation of the methyl group about the C_9C_{10} bond. For the calculation of the associated partition function, this internal motion will be treated as a hindered internal rotor. All other low vibrational motions will be treated in the harmonic oscillator approximation.

Torsional Potentials. The torsional potential for the methyl rotation in the TSC5 conformer has a period of $\pi/3$. The strong repulsive interaction between the hydrogens of the methyl group and the phenyl π cloud gives rise to relatively large rotational barriers. The symmetry number in this case is 3 ($\sigma_{int} = 3$). The results of the Fourier fitting procedure are listed in Table 3.

3.2.3. Product State. Geometries. The optimized structure for the product state is shown in Figure 9 and will be referred as

TABLE 3: Geometrical Parameters and Rotational Potentials for the Internal Rotations[a]

			Fourier fit results			
ab inito calculations		E_{rel}^0	I_m	V_i		
Internal Rotations in the Secondary Butylbenzene Radical						
	ϕ_1	rotation about the C_1-C_7 bond				ϕ_1^f
BBsec1	0.0	0.0	123.61	V_2	5.959	0.0
	86.52	5.94				90.0
	ϕ_2	rotation about the C_7-C_8 bond				ϕ_2^f
BBsec1	0.0	0.0	185.08	V_1	6.928	0.0
TSBBsec1−BBsec2	59.5	13.27		V_2	−3.595	61.4
BBsec2	116.2	2.24		V_3	14.231	115.9
TSBBsec2−BBsec2	179.5	21.16				180.0
	ϕ_3	rotation about the C_8-C_9 bond				ϕ_3^f
BBsec1−BBsec1	0.0	0.26	85.46	V_1	4.485	
BBsec1	6.9	0.0		V_2	−2.502	
BBsec1−BBsec3	52.0	1.61		V_3	2.403	66.0
BBsec3	89.7	0.95				117.7
BBsec3−BBsec3	180.0	6.89				
	ϕ_4	rotation about the C_9-C_{10} bond				ϕ_4^f
BBsec1	0.0	0.0	11.04	V_3	2.031	0.0
	75.1	1.73				60.0
Internal Rotations in the Transition State						
		methyl rotation				
	ϕ_4					ϕ_4^f
TSC5	0.0	0.0	11.17	V_3	8.913	0.0
	66.354	8.669				60.0
Internal Rotations in the Product State						
		methyl rotation				
PR5	0.0	0.0	11.17	V_3	12.211	0.0
	60.474	12.21				60.0

[a] E_0^{rel} is the relative energy (kJ/mol) with respect to that of the reference conformers for the secondary butylbenzene radical BBsec1, the transition state TSC5, and the product state PR5. V_i is expressed in kJ/mol. The angles are relative to the equilibrium values of the reference conformers. ϕ_1^f, ϕ_2^f, θ_3^f, and ϕ_4^f are the angles as obtained from the Fourier fitting procedure. I_m is the reduced moments of inertial (au) for each individual rotation.

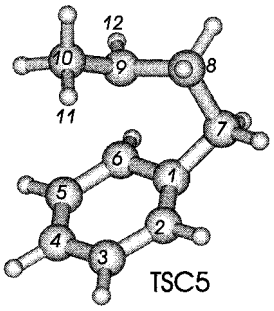

Figure 8. Transition state for cyclization of the secondary butylbenzene radical.

the PR5 conformer. This is a fused ring system of a five- and six-membered ring. The aromaticity of the former benzene ring is broken an accordingly the six-membered ring deviates from planarity ($C_2C_1C_6C_5 = 10.874°$, $C_6C_5C_4C_3 = 4.353°$, $C_5C_4C_3C_2 = 4.416°$, $C_4C_3C_2C_1 = -5.048°$, $C_3C_2C_1C_6 = -3.060°$). The conjugated π-system can only be re-established after hydrogen abstraction at the center C_6. Additionally, the carbon C_1 transforms from a tetrahedral center toward a radical center during the cyclization reaction. Therefore, it evolves to an almost planar sp^2 center (improper torsion angle $C_6C_1C_2C_7 = -172.227°$).

Vibrational Analysis. The PR5 conformer has a set of low vibrational frequencies: $\nu_b = 74.0$, $\nu_{sk1} = 131.7$, $\nu_{sk2} = 186.4$ and $\nu_4 = 230.2$ cm^{-1}. The ν_b frequency can be identified with a bending motion of the two fused ring systems toward each other. ν_{sk1} and ν_{sk2} are skeletal motions. Only ν_4 corresponds to a pure internal rotation of the methyl group about the C_9C_{10} bond and will be treated as a hindered internal rotor.

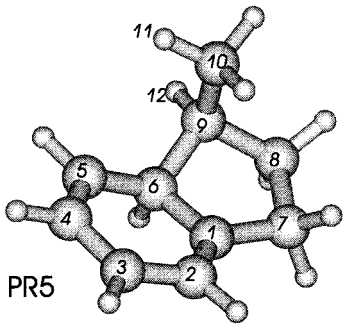

Figure 9. Product state for cyclization of the secondary butylbenzene radical.

Torsional Potentials. The rotational potential for the methyl rotation in the PR5 conformer has a period of $\pi/3$ and a symmetry number of $\sigma_{int} = 3$ is taken into account for the evaluation of the partition function. The results of the Fourier fitting procedure are listed in Table 3, and the rotational potential is shown in Figure 10b.

3.3. Activation Energies and Rate Constants. The ab initio calculations on the different cyclization pathways for the butylbenzene radical are able to yield reliable predictions for the kinetic parameters. Total binding energies and zero-point vibrational energies of all reactants, transition states, and products are taken up in Table 4. The microscopically determined partition functions serve as a bridge to the macroscopic kinetic parameters. They are calculated for all species at temperatures ranging from 100 to 1000 K. By means of the rate equation (eq 1) of TST, we are able to construct Arrhenius plots for the reactions under study. They are displayed in Figure 11. A and E_a are now determined by fitting a linear function through the data points by means of a least-squares method. The slope of this best-fit line gives the activation energy while the intercept leads to the pre-exponential factor. The results are listed in Table 4.

3.3.1. Influence of Internal Rotations on the Reaction Rates. The activation energy is largely determined by the molecular energy difference at the absolute zero between activated complex and reactant. The influence on the activation energies by a correct treatment of internal rotations is rather small in this case. The shift amounts to 0.14 kJ/mol for the cyclization of the BB1 conformer and to −0.696 kJ/mol and −0.03 kJ/mol for the forward and reverse cyclization reaction of the secondary butylbenzene radical. Two main effects are responsible for these shifts:

(i) In the internal rotor approach, the molecular energy difference ΔE_0 has to be corrected with the ZPE's of those vibrations which stand for the internal rotations. These ZPE's may differ substantially from the ZPE's of the internal rotations (given by the deepest bound rotational levels). If this happens, it may affect the activation energy in a considerable way.

(ii) The level density of the rotational potential may increase in most of the cases. This has a direct impact on the rotational partition functions. For the reaction BB1 → PR6, the effect of the partition functions on the activation energy is −1.4 kJ/mol in the harmonic oscillator (HO) approach versus −2.96 kJ/mol in the internal rotor (IR) approach. However, the global effect on E_a is small since both previous mentioned effects nearly cancel each other.

The impact of internal rotations on the pre-exponential factor is large. The ratio A^{HO}/A^{IR} amounts to 9.3 and 6.4 for the

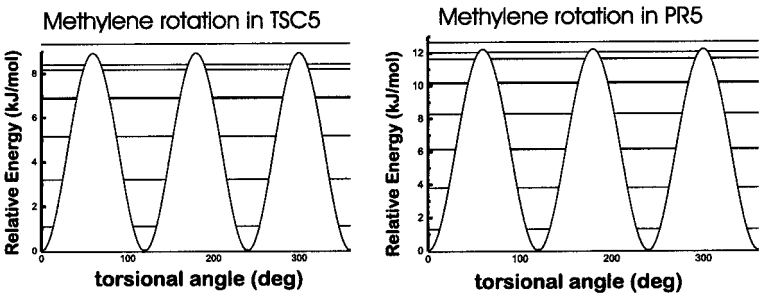

Figure 10. Rotational potentials for the torsional motions in the TSC5 and PR5 conformer. The energies are relative with respect to those of the TSC5 and PR5 conformers. The torsional angles are relative with respect to the equilibrium geometry of the TSC5 and PR5 conformers.

TABLE 4: Energies and Kinetic Characteristics[a]

Cyclization of the Primary Butylbenzene Radical			
	BB1	TSC6	PR6
E_0 (au)	−388.935907	−388.917564	−388.949337
ZPE (au)	0.193232	0.193691	0.196281
	forward reaction	reverse reaction	
ΔE_0 (kJ/mol)	49.36	76.53	
$\Delta E'_0$ (kJ/mol)	51.06		
E_a^{HO} (kJ/mol)	47.96	78.74	
A^{HO}	4.3×10^{10}	3.3×10^{13}	
E_a^{ir} (kJ/mol)	48.10		
A^{ir}	4.6×10^{9}		

Cyclization of the Secondary Butylbenzene Radical			
	BBsec1	TSC5	PR5
E_0 (au)	−388.942237	−388.913069625	−388.939245
ZPE (au)	0.193735	0.194807	0.196571
	forward reaction	reverse reaction	
ΔE_0 (kJ/mol)	79.39	64.09	
$\Delta E'_0$ (kJ/mol)	79.82	64.25	
E_a^{HO} (kJ/mol)	77.85	66.17	
A^{HO}	4.3×10^{10}	2.7×10^{13}	
E_a^{ir} (kJ/mol)	77.15	66.14	
A^{ir}	6.7×10^{9}	2.8×10^{13}	

[a] E_0 is the total binding energy of the groundstate configuration, zero-point vibration energies ZPE are scaled with 0.9806,[27] and ΔE_0 is the molecular energy difference (ab initio DFT) between the transition state and the reactants with the inclusion of ZPE. $\Delta E'_0$ represents ΔE_0 with the ZPE of those vibrations which stand for internal rotations subtracted. E_a^{HO} and A^{HO} are the activation energy and the preexponential factor calculated with all vibrational motions treated within harmonic oscillator approximation, while E_a^{IR} and A^{IR} are equivalent quantities calculated with explicit consideration of internal rotations and corrected for the corresponding ZPE. A is expressed in units of s^{-1}.

reactions BB1 → PR6 and BBsec1 → PR5, respectively. This can entirely be attributed to the role of the partition functions. For this particular reaction, the frequency factor decreases by implementing internal rotations, whereas for the addition reaction (see Figure 1a and ref 10), we found an increase. This can be understood by studying the explicit form of the rate constant (eq 1). In the addition reaction, the partition function of the species which is most drastically affected (this is the transition state) figures in the nominator, while in the cyclization reaction, the partition function of the butylbenzene radical, which in turn is most affected by IR's, figures in the denominator as reactant.

The level density is largely increased when going from the HO to the IR toward the free-rotor case. This can lead to a serious enhancement of the partition functions. The relative increase depends on the strength of the potential compared with the inertial moments of the rotating groups ($\hbar^2/(2I_m)$). For the reverse reaction PR5 → BBsec1, the influence is rather small due the large rotational barriers of the methyl rotation (Figure 10). Moreover, the methyl rotations in both the TSC5 and PR5 conformer compensate each other in the evaluation of the rate constant. For both forward cyclization reactions, the effect is large. By treating the internal rotations as vibrations, one gets stuck in the potential well of the reference conformer due to the infinite walls of an HO potential. In our case, the BB1 (the most symmetrical conformer as defined in ref 10) and BBsec1 are taken as reference conformers, and as a result, all other stable structures on the potential energy surface (BB1, BB2, BB3, BB4, BBsec2, BBsec3, BBsec4, and BBsec5) cannot be reached in this picture. In the IR approach, all conformers are accessible, and the number of states in which the molecule can reside due to thermal agitation is much larger, leading to a serious increase of the partition functions. In principle, one should consider coupled internal rotations to take into account conformers like BBsec4 and BBsec5 properly, since these structures can only be reached by a path through a two-dimensional rotational surface. For this extension, we refer to ref 34.

3.3.2. Relative Importance of Five- and Six-Membered Ring Formation. In this subsection, we want to link our microscopic results for the cyclization pathways with macroscopic aspects of coke formation in an industrial cracking unit. Figure 12 shows the kinetic network for the cyclization reaction and the following steps that ultimately lead to a further growth of the coke layer. The isomerization of the primary to the secondary butylbenzene radical occurs via successive hydrogen abstractions. The cyclization is assumed to be the rate-determining step since the subsequent dehydrogenation reaction which eventually results in a new aromatic ring is much faster than the reverse ring opening reaction. On the basis of these assumptions, the relative rate of formation of a six-membered to a five-membered ring can be written as

$$\frac{R_{6-\text{ring}}}{R_{5-\text{ring}}} = \frac{k_1\, C_{\text{BB1}}}{k_2 C_{\text{BBsec1}}} \tag{7}$$

To validate the importance of six-membered and five-membered ring formation, we must take both the thermodynamic and kinetic aspects into consideration. For the thermodynamic part, we refer to Figure 13, where the energy diagram for the cyclization reactions is given. When comparing the ground-state energies of the BB1 and BBsec1 radical, it follows that the secondary radical is stabilized by 16.6 kJ/mol over the primary one, as expected. If the two radicals were in equilibrium, this would mean that the secondary radical would be present in much higher concentrations than the primary one, especially at low temperatures. The ratio of the two radical concentrations converges to a small value at high temperatures (approximately

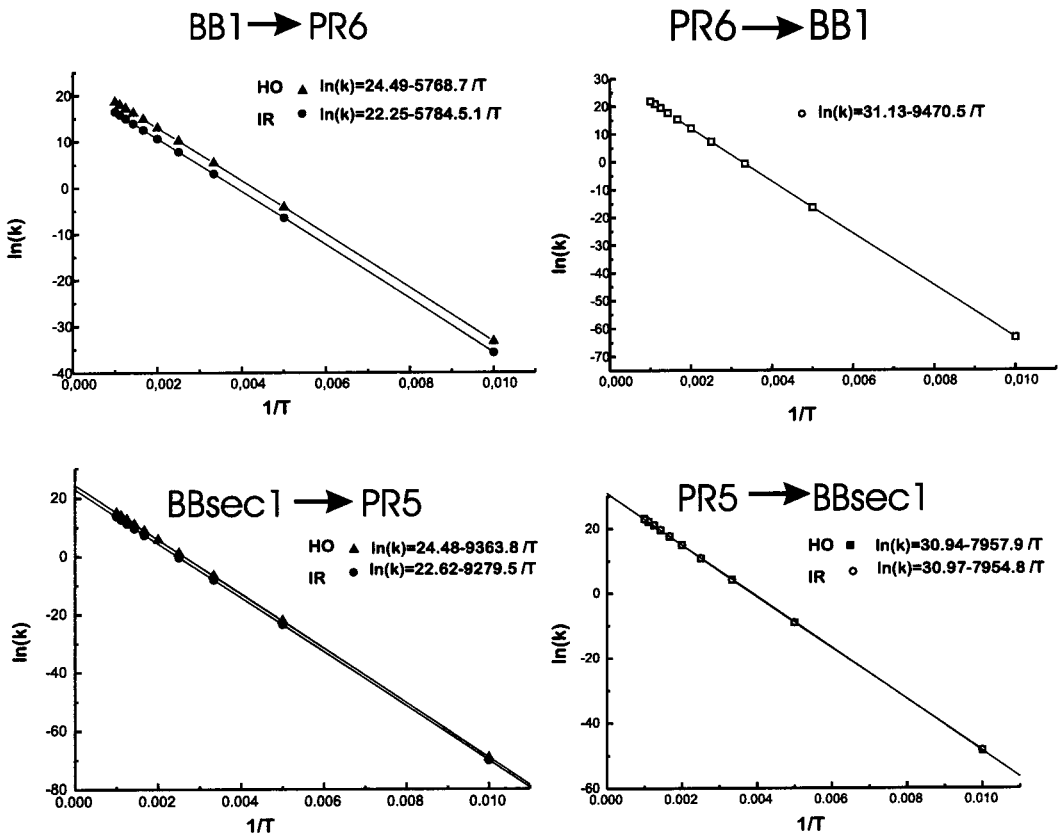

Figure 11. Arrhenius plots of ln k vs $1/T$ for the different cyclization reactions.

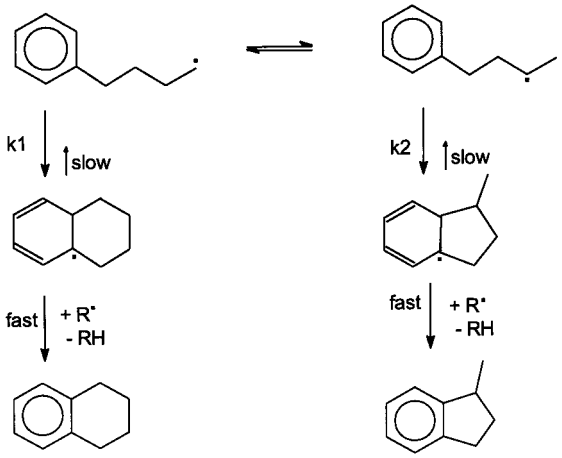

Figure 12. Kinetic network for the cyclization of the butylbenzene radical.

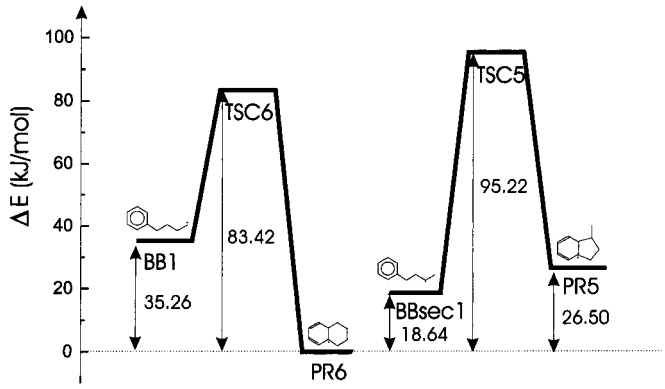

Figure 13. Energy diagram for the cyclization reactions. All energies are relative to the ground-state energy of the PR6 conformer (−388.949337 au). The energy differences do not include ZPE.

5 at 1000 K). When comparing the ground-state energies of the PR5 and PR6 conformer, it follows that the fused ring system of two six-membered rings is stabilized by 26.5 kJ/mol. Since both radicals are tertiary radicals, this effect can be traced back to the additional ring strain present in a five ring. Benson[3] gives a value of 26.4 kJ/mol for the ring strain in a five-membered ring, in excellent agreement with our value.

To have an idea about the relative concentrations of primary and secondary radical in an industrial cracking unit, we performed a simulation of the concentration profiles inside the coils of a typical industrial nafta cracking unit with a simulation program, based on a detailed network of elementary reactions, developed at the Laboratorium voor Petrochemische Techniek.[1,2] At the beginning of the reactor, primary radicals dominate since they are preferably formed by β-scission reactions of higher-molecular-weight nonbranched alkyl radicals or from branched radicals, where the radical position is at the branching position. The consecutive reactions responsible for formation of secondary radicals are not fast enough to establish equilibrium between the two radicals. It is only at the end of the reactor at very high temperatures (1000−1200 K) that the ratio of secondary to primary radicals increases to values between 1 and 1.5, i.e., still below the equilibrium ratio. At the high temperatures encountered at the end of the reactor, the favoring thermodynamic aspects of the secondary radicals are still of minor importance. Hence, the ratio of the rate coefficients determines the relative importance of five- and six-membered ring formation for coke formation in a thermal cracking unit.

The ratio of the rate of six-membered to five-membered ring formation is dependent on the ratio of the rate coefficients for cyclization (eq 7). From Table 4, it can be seen that the preexponential factors are very similar; however, the activation energy for the six-membered ring formation is 30 kJ/mol lower

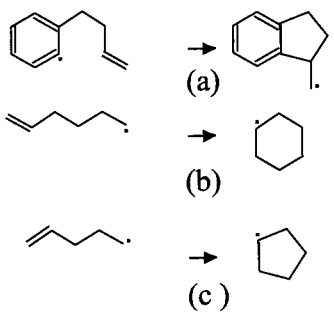

Figure 14. Schematic representation of some radical reactions.

than that for the five-membered ring formation. At 300 K, the ratio of the rate coefficients is 80 000, and at 1000 K, it is still 23. From this, it is reasonable to state that formation of six-membered rings is preferred over formation of five-membered rings under typical steam cracking conditions.

Recently Jursic[35] and Olivella et al.[36] studied the cyclization pathways for the hexenyl radical toward five- and six-membered rings. They found that there can only be a kinetic preference for five-membered rings over six-membered ones if there is an additional stabilizing effect for the transition state such as π-bond participation that is properly positioned in the molecule.[37−39,40−42] This feature would be present in the cyclization reaction of the 2-(3-butenyl)phenyl radical, as displayed in Figure 14a. In this case, preferable interactions occur between the p-molecular orbitals of the butenyl chain and the singly occupied phenyl radical orbital. Because of this additional stabilizing effect, it is reasonable to expect that the activation energy for this cyclization reaction should be very low. Experimentally, a value of 15.06 kJ/mol was estimated for this reaction,[33] and theoretical values at the B3LYP/6-31G-(d) level predict an activation energy of 12.13 kJ/mol.[35] However, the reactant radical, as displayed in Figure 14a, is not likely to be an important intermediate in the formation of coke. Cyclization at the coke surface occurs rather from radicals positioned in the alkylchain attached to the already formed coke layer.

3.3.3. Validation with Experimental Results. For the reactions under study, no experimental results are available, and hence, a direct comparative study of theoretical predicted values for A and E_a is excluded. As an alternative, we can compare our results with similar radical cyclization reactions. For the formation of six-membered rings, we can compare with the cyclization reaction of the hexenyl radical toward the cyclohexyl radical, as schematically displayed in Figure 14b. Values of 34.995 kJ/mol for the activation energy and $1\times10^{10}s^{-1}$ for the preexponential factor are reported by Handford et al.[43] For five-membered ring formation, we compare with the cyclization reaction of the pentenyl radical toward the cyclopentyl radical (Figure 14c). Gierczak et al.[44] report values of 67.779 kJ/mol for the activation energy and 1.41×10^{11} for the frequency factor.

The experimental values confirm the preference for six-membered ring formation over five-membered one in the case where additional π-bond participation is not present. The activation energy for the cyclization of the hexenyl radical is approximately 33 kJ/mol lower than the corresponding reaction for the pentenyl radical. This difference in activation is in close agreement with our theoretical predicted values and is an indication for the relative importance of both pathways.

For both reactions, the theoretical predicted activation energies are higher than the experimental ones. This can probably be traced back to the extra steric hindrance due to the presence of the aromatic ring in the considered reactions. Our values are probably good estimates for the real experimental values since the relative stabilization of five and six-membered rings is in close agreement with each other.

The theoretical estimates for the frequency factor are on the same order of magnitude as the experimental values, confirming the assumption that the B3LYP/6-311G** predictions provide reasonable values for the kinetic parameters.

4. Conclusions

In this paper, we have studied some main reactions of the coke formation network, namely, different cyclization pathways for the butylbenzene radical. These reactions can lead to a further growth of the coke layer. Both primary and secondary butylbenzene radicals can be expected to be present. They can undergo cyclization toward either a five- or six-membered ring. The relative importance of both pathways is studied by calculating theoretical values for the relevant kinetic parameters.

In the first part, a detailed conformational analyses is performed on the DFT/B3LYP/6-311G** level of all products, reactants, and transition states. This method is known to give reliable predictions of geometries, frequencies, and energies for radical reactions.[19,8] All stable conformers of reactants, products, and transition states have been located by full geometry optimizations. This was followed by a detailed vibrational analyses of all species. Some low-vibrational modes were identified as internal rotations. They were treated in an exact quantum-mechanical way by solving the appropriate one-dimensional Schrödinger equation with a rotational potential determined from our ab initio calculations. The obtained rotational energy eigenvalues serve as an input for the microscopic partition functions.

In the second part, the molecular partition functions, determined in a microscopic way, serve as a bridge for macroscopic kinetic quantities such as the preexponential factor and activation energy. The influence of internal rotations on these Arrhenius parameters has been studied in detail. It is found that the influence on the activation energy by treating internal rotations properly is rather small. This quantity is mainly determined by the molecular energy difference at the absolute zero between the activated complex and reactant. The frequency factor on the other hand is largely affected by the method of constructing the partition functions. For both forward cyclization reactions, the pure effect of internal rotations decreases the preexponential factor by a factor of 9 and 6. This could be expected since the level density of the eigenstates is substantially increased in the IR versus the HO approach. As a result, the molecule can reside in more stable conformers due to thermal agitation.

In addition, the kinetic parameters predict an activation energy that is approximately 30 kJ/mol lower for the formation of six-membered rings with respect to five-membered rings. Moreover, the product formed from the primary butylbenzene radical is largely stabilized over the fused ring system with a five-membered ring. Studies of concentration profiles of secondary and primary radicals in an industrial cracking unit teach that the relative importance of five- and six-membered ring formation is primarily determined by the rate coefficients of both cyclization pathways. The kinetic aspects support the assumption that the formation of six-membered rings is preferred over the formation of five-membered rings under typical steam cracking conditions.

Finally, our kinetic parameters are compared with experimental values. Since, however, there are no direct data available for the reactions under consideration, comparison is made with similar cyclization reactions of the hexenyl and pentenyl

radicals. The difference in experimentally determined activation energies for the formation of five- and six-membered rings is in very good agreement with the corresponding to theoretical value. Also, the frequency factors are within the same order of magnitude. Therefore, it can be expected that our theoretical estimates for the kinetic parameters determined at the B3LYP/6-311G** level of theory are in good agreement with experiment.

The calculations as presented here are especially important for gaining insight into elementary reactions of the thermal cracking and coke formation network, since in this case it is very difficult to obtain experimental information on individual reactions. Ab initio calculations can enable us to validate important assumptions of the kinetic model of the coke formation.

Acknowledgment. This work is supported by the Fund for Scientific Research - Flanders (FWO) and the Research Board of Ghent University.

Note Added after ASAP Posting. This paper was first published on the web with uncorrected errors on 7/12/01. The correct version appeared on 7/23/01.

References and Notes

(1) Clymans, P. J.; Froment, G. F. *Comput. Chem. Eng.* **1984**, *8*, 137−142.

(2) (a) Reyniers, G. C.; Froment, G. F.; Kopinke, F. D.; Zimmerman, G. *Ind. Eng. Chem. Res.* **1994**, *33* (11), 2584−2590. (b) Plehiers, P. M.; Reyniers, G. C.; Froment, G. F. *Ind. Eng. Chem. Res.* **1990**, *29*, 636−641.

(3) Benson, S.W. *Thermochemical kinetics*; Wiley: New York, 1976.

(4) (a) Eyring, H. *J. Chem. Phys.* **1935**, 107. A more comprehensive treatment can be found in Wynne-Jones, W. F. K.; Eyring, H. *J. Chem. Phys.* **1935**, 3, 492. This article is reproduced in full in Back, M. H.; Laidler, K. L. *Selected Readings in Chemical Kinetics*; Pergamon: Oxford, 1967. (b) Evans, M. G.; Polanyi, M. *Trans. Faraday Soc.* **1935**, *31*, 875, **1937**, *33*, 448. (c) Laidler, K. J. *Chemical kinetics*; HarperCollins: New York, 1987. (d) Mc. Quarrie, D. A.; Simon, J. D. *Physical Chemistry-A Molecular Approach*; University Science Books: Sausalito, CA, 1997. (e) For reviews, see for example: (i) Pechukas, P. In *Dynamics of Molecular Collisions, Part B*; Miller, W. H., Ed.; Plenum Press: New York, 1976. (ii) Laidler, K. J.; King, M. C. *J. Phys. Chem.* **1983**, *87*, 2657. (iii) Truhlar, D. G.; Hase, W. L.; Hynes, J. T. *J. Phys. Chem.* **1983**, *87*, 2664. (iv) Gilbert, R. G.; Smith, S. C. *Theory of Unimolecular and Recombination Reactions*; Blackwell: Oxford, 1990.

(5) (a) Willems, P. A.; Froment, G. F. *Ind. Eng. Chem. Res.* **1988**, *27*, 1959−1966. (b) Willems, P. A.; Froment, G. F. *Ind. Eng. Chem. Res.* **1988**, *27*, 1966−1971.

(6) Heuts, J. P. A.; Gilbert, R. G.; Radom, L. *J. Phys. Chem.* **1996**, *100*, 18997−19006.

(7) Heuts, J. P. A.; Gilbert, R. G.; Radom, L. *Macromolecules* **1995**, *28*, 8771−8781.

(8) Smith, D. M.; Nicolaides, A.; Golding, B. T.; Radom, L. *J. Am. Chem. Soc.* **1998**, *120*, 10223−10233.

(9) Richter, H.; Mazyar, O. A.; Sumathi, R.; Green, W.; Howard, J. B.; Bozzelli, J. W. *J. Phys. Chem. A* **2001**, *105* (9), 1561.

(10) Van Speybroeck, V.; Van Neck, D.; Waroquier, M.; Wauters, S.; Saeys, M.; Marin, G. *J. Phys. Chem. A* **2000**, *104*, 10939−10950.

(11) Wauters, S.; Marin, G. B. *Chem. Eng. J.* **2001**, *82* (1-3), 267.

(12) Gang, J.; Pilling, M. J.; Robertson, S. H. *J. Chem. Soc., Faraday Trans.* **1996**, *92* (19), 3509−3518.

(13) For an example of a reference work, see: Parr, R. G.; Yang, W. *Density-Functional Theory of Atoms and Molecules*; Oxford University Press: Oxford, 1989.

(14) Fessenden, R. J.; Fessenden, J. S. *Organic Chemistry*; Brooks/Cole Publishing Company: Pacific Grove, CA, 1990.

(15) Van Speybroeck, V.; Martelé, Y.; Waroquier, M.; Schacht, E. *J. Am. Chem. Soc*, submitted for publication.

(16) Frisch, M. J.; Trucks, G. W.; Schlegel, H. B.; Scuseria, G. E.; Robb, M. A.; Cheeseman, J. R.; Zakrzewski, V. G.; Montgomery, J. A.; Stratmann, R. E., Jr.; Burant, J. C.; Dapprich, S.; Millam, J. M.; Daniels, A. D.; Kudin, K. N.; Strain, M. C.; Farkas, O.; Tomasi, J.; Barone, V.; Cossi, M.; Cammi, R.; Mennucci, B.; Pomelli, C.; Adamo, C.; Clifford, S.; Ochterski, J.; Petersson, G. A.; Ayala, P. Y.; Cui, Q.; Morokuma, K.; Malick, D. K.; Rabuck, A. D.; Raghavachari, K.; Foresman, J. B.; Cioslowski, J.; Ortiz, J. V.; Baboul, A. G.; Stefanov, B. B.; Liu, G.; Liashenko, A.; Piskorz, P.; Komaromi, I.; Gomperts, R.; Martin, R. L.; Fox, D. J.; Keith, T.; Al-Laham, M. A.; Peng, C. Y.; Nanayakkara, A.; Gonzalez, C.; Challacombe, M.; Gill, P. M. W.; Johnson, B.; Chen, W.; Wong, M. W.; Andres, J. L.; Gonzalez, C.; Head-Gordon, M.; Replogle, E. S.; Pople, J. A. *Gaussian 98*, Revision A.7; Gaussian, Inc.: Pittsburgh, PA, 1998.

(17) Becke, A. D. *J. Chem. Phys.* **1993**, *98*, 5648.

(18) Krishnan, R.; Binkley, J. S.; Seeger, R.; Pople, J. A. *J. Chem. Phys.* **1980**, *72*, 650.

(19) Wong, M. W.; Radom, L. *J. Phys. Chem. A* **1998**, *102*, 2237−2245.

(20) Parker, C. L.; Cooksy, A. L. *J. Phys. Chem. A* **1998**, *102*, 6186−6190.

(21) Lynch, B. J.; Fast, P. L.; Harris, M.; Truhlar, D. G. *J. Phys. Chem. A* **2000**, *104*, 4811−4815.

(22) Ochterski, J. W.; Petersson, G. A.; Montgomery, J. A. *J. Chem. Phys.* **1996**, *104*, 2598−2619.

(23) Curtiss, L. A.; Raghavachari, K.; Trucks, G. W.; Pople, J. A. *J. Chem. Phys.* **1991**, *94*, 7221−7230.

(24) Mayer, P. M.; Parkinson, C. J.; Smith, D. M.; Radom, L. *J. Chem. Phys.* **1998**, *108*, 604−615.

(25) Peng, C.; Ayala, P. Y.; Schlegel, H. B.; Frisch, M. J. *J. Comput. Chem.* **1996**, *17*, 49.

(26) Peng, C.; Schlegel, H. B. *Isr. J. Chem.* **1994**, *33*, 449.

(27) Scott, A. P.; Radom, L. *J. Phys. Chem.* **1996**, *100*, 16502−16513.

(28) Lister, D. G.; MacDonald, J. N.; Owen, N. L. *Internal Rotation and Inversion*; Academic Press: London, 1978. Kroto, H. W. *Molecular Spectra*; Dover Publications: New York, 1992.

(29) Hehre, W. J.; Radom, L.; Schleyer, P. v. R.; Pople, J. A. *Ab Initio Molecular Orbital Theory*; Wiley: 1986.

(30) Viskolcz, B.; Lendvay, G.; Seres, L. *J. Phys. Chem. A* **1997**, *101*, 7119−7127.

(31) Kerr, J. A. *Chem. Rev.* **1966**, *66*, 465.

(32) Pryor, W. A.; Fuller, D. L.; Stanley, J. P. *J. Am. Chem. Soc.* **1972**, *94*, 1632.

(33) Johnson, L. J.; Lusztyk, J.; Wayner, D. D. M.; Abeywickreyma, A. N.; Beckwith, A. L.; Scaiano, J. C.; Ingold, K. U. *J. Am. Chem. Soc.* **1985**, *107*, 4594.

(34) Van Speybroeck, V.; Van Neck, D.; Waroquier, M. *J. Chem. Phys.*, submitted for publication.

(35) Jursic, B. S. *J. Mol. Struct. (THEOCHEM)* **1999**, *492*, 285−291.

(36) Olivella, S.; Sol'e, A. *J. Am. Chem. Soc.* **2000**, *122*, 11416−11422.

(37) Beckwith, A. L. J.; Eaton, C. J.; Serelis, A. K. *J. Chem. Soc. Chem. Commun.* **1980**, 482.

(38) Beckwith, A. L. J.; Laurence, T.; Serelis, A. K. *J. Chem. Soc. Chem. Commun.* **1980**, 484.

(39) Beckwith, A. L. J. *Tetrahedron* **1981** *37*, 3073.

(40) Dewar, M. J. S.; Olivella, S. *J. Am. Chem. Soc.* **1978**, *100*, 5290.

(41) Spellmeyer, D. C.; Houk, K. N. *J. Org. Chem.* **1987** *52*, 959.

(42) Beckwith, A. L. J.; Schiesser, C. H. *Tetrahedron* **1985**, *41*, 3925.

(43) Handford-Styring, S. M.; Walker, R. W. *J. Chem. Soc. Faraday Trans.* **1995**, *91*, 1431−1438.

(44) Gierczak, T.; Gawlowski, J.; Niedzielski, J. *Int. J. Chem. Kinet.* **1986**, *18*, 623−637.